Physics of the Solid State, 2025, Vol. 67, No. 2

11,16

Kinetics of fragmentation of endohedral metallofullerene clusters in a polar solvent

© E.K. Alidzhanov[1], I.E. Kareev[2], V.P. Bubnov[2], A.I. Kotov[2], S.N. Letuta[1], Yu.D. Lantukh[1], D.A. Razdobreev[1]

[1] Orenburg State University,
Orenburg, Russia
[2] Federal Research Center of Problems of Chemical Physics and Medicinal Chemistry RAS,
Chernogolovka, Russia

E-mail: kareev@icp.ac.ru

Received November 11, 2024
Revised December 23, 2024
Accepted December 24, 2024

The evolution of the morphology of endohedral metallofullerene La@C_{82} clusters in N, N-dimethylformamide with the addition of diethylamine was studied using dynamic and static light scattering methods. It was found that the addition of diethylamine to a solution of endohedral metallofullerene leads to a decrease in the effective value of the hydrodynamic radius of clusters from 100 to 35 nm, and the intensity of light scattering of the solution decreases by 30 times, provided that its molar concentration remains constant. The fractal dimension of La@C_{82} clusters at the initial and final stages of their fragmentation was estimated from the analysis of the angular and concentration dependences of light scattering of endohedral metallofullerene solutions. The results of measurements of the time evolution of the light scattering intensity and the hydrodynamic radius of endohedral metallofullerene clusters formed the basis for assessing the fragmentation rate of EMF clusters.

Keywords: endohedral metallofullerenes, clusters, cluster fragmentation rate, dynamic and static light scattering.

DOI: 10.61011/PSS.2025.02.60688.302

1. Introduction

Unique structure of endohedral metallofullerenes (EMF), diversity of their chemical and physical properties attract great interest among researchers [1]. EMF might be used as molecular conductors, magnetics, ferroelectrics and contrast materials for NMR tomography. EMF might be used very effectively in nuclear medicine and tomography [2,3]. However, physical and particularly chemical properties of EMF are still poorly understood.

It is known that EMF form large aggregates ($R \approx 100\,\mathrm{nm}$) in polar solvents, and these aggregates have a negative effective charge characterized by high zeta potential $\xi \approx -26\,\mathrm{mV}$ [4]. Zeta potential is one of the key properties of an electrical double layer (EDL) that appears in contact of two colloidal solution phases. With increasing ionic strength of the solvent (for example, when hydrochloric acid is added), decrease in the absolute zeta potential is observed and colloidal particles get larger [5,6]. For EDL depletion, high ($\sim 0.5\,\mathrm{M}$) concentrations of chloride anions are required.

In addition to supporting electrolytes (e.g. HCl), colloid destabilization may be induced by ions that selectively react with particular areas on the surface of colloidal particles. In [6,7], it is shown that aluminum oxide suspensions are aggregated in the presence of less than $10^{-3}\,\mathrm{M}$ sodium sulfate, whose anions are bound specifically with oxide molecules and neutralize the repulsion forces acting between colloidal particles. Chorover et al. [8] describe the hematite aggregation process induced by specific phosphate adsorption with extremely low ($10^{-3}\,\mathrm{M}$) concentration.

Fullerenes and their derivatives are good electron acceptors and form charge-transfer complexes with nitrogen-containing molecules [9]. The study of electronic absorption spectra of La@C_{82} anions and cations in [10] showed that EMF oxidation and reduction take place via addition or loss of an electron from the carbon cage. As established in [11], nitrogen-containing solvent molecules form charge-transfer complexes with EMF molecules by transferring the latter into the anionic state.

Thus, specific interaction between EMF molecules and nitrogen-containing molecules may disturb thermodynamic equilibrium of the colloidal system, thus, causing its evolution. Key parameters characterizing such process include free Gibbs energy, corresponding variations of enthalpy ΔH and entropy ΔS, equilibrium aggregation constants K of a colloidal system [12].

Recently, with evolvement of nanotechnologies, a special focus has been made on the identification of fundamental laws and physical and chemical features of synthesis of nanoscale structures with desired properties. Static and dynamic light scattering [13], electronic and atomic-force microscopy [14,15] are used as the main high-sensitivity methods for nanostructure control.

Earlier in [5], the authors studied in detail the La@C_{82} cluster aggregation process with addition of HCl as a coagulant. This study investigates experimentally the fragmentation process of La@C$_{82}$ EMF clusters in a polar solvent solution with addition of 10^{-5} M diethylamine. Key characteristics of EMF dissociation and aggregation processes are determined directly from the experimental dynamic and static light scattering data.

2. Experiment procedure

Soot containing EMF with lanthanum was prepared by composite graphite electrode evaporation in an arc reactor developed and fabricated by us [16,17]. EMF was extracted from the soot by *o*-dichlorobenzene (≥ 99 % (GC), Sigma-Aldrich) in argon atmosphere at the solvent boiling temperature. Isomerically pure La@C$_{82}$(C_{2v}) EMF was prepared by the multistage semi-preparative high performance liquid chromatography (HPLC) with successive use of Cosmosil Buckyprep (10×250 mm) and Riges Buckyclutcher (10×250 mm) columns with two types of sorbents. Toluene (ACS) was used as an eluent, UV detector wavelength was 310 nm. La@C$_{82}$ EMF (C_{2v} isomer) in toluene was characterized according to a procedure described in detail in [18].

La@C$_{82}$ stock solution in *N*, *N*-dimethylformamide (DMF, C.P., EKOS-1, Russia) with the pre-defined concentration was prepared in argon using the following procedure. EMF was accurately weighed on an analytic balance and then diluted in 3 mL of solvent. DMF was pre-distilled in vacuum, and solvent purity was confirmed by the absence of amine-based impurities.

The EMF solution was subjected to ultrasonic treatment at 40 °C. A vial with solution was held for several days at room temperature for precipitation of undissolved EMF. Solution monodispersity was controlled by dynamic light scattering method. The top of solution was placed into a clean vial. Solvent was evaporated from the undissolved precipitate. Then, the EMF residue was weighed. Solvent concentration was calculated from the weight of dissolved EMF and the volume of solvent. Solvent concentration was further changed by dilution. EMF concentration in the solution was controlled additionally through the optic absorption spectra and the known molar extinction coefficient of La@C$_{82}$ [19] at 630 nm.

Fragmentation of the La@C$_{82}$ clusters in the DMF solution ($C_0 = 1.5 \cdot 10^{-5}$ M) was studied by the dynamic and static light scattering methods. Fragmentation of EMF clusters was induced by adding 5 μL diethylamine to the EMF (2 mL) stock solution. Diethylamine molecules form charge-transfer complexes with EMF molecules by transferring the latter into the anionic state [11]. This probably reduces intermolecular dipole-dipole interaction in the EMF clusters, thus, promoting their fragmentation.

The dynamic light scattering (DLS) method was used to study the kinetic dependence of EMF nanocluster distribution over the hydrodynamic radii. Measurements were carried out using the Photocor Compact-Z analyzer with the scattering angle of 90 °. $\lambda = 654$ nm semiconductor laser was used as a light source. This instrument was also used to measure light scattering intensity variation kinetics.

Fractal dimension of the EMF clusters D_f was measured by multi-angle (40–130 °) static light scattering (SLS) method using an in-house system with helium-neon laser ($\lambda = 632$ nm) and PMT complete with an interference filter.

3. Experimental results and discussion

For the La@C$_{82}$ stock solution, the DLS methods was used to establish that the EMF cluster distribution was relatively monodispersed with a mean hydrodynamic radius of $R_0 \approx 100$ nm (Figure 1, *a*). For large clusters $R > q^{-1}$, the angular dependence of light scattering intensity is written as [20]:

$$I(q) \propto (qR)^{-D_f}, \quad (1)$$

here, $q = 4\pi n \sin(\Theta/2)/\lambda$ is the module of scattering wave vector, D_f is the fractal dimension of clusters.

Thus, by measuring the angular dependence of light scattering intensity of the EMF stock solution and repre-

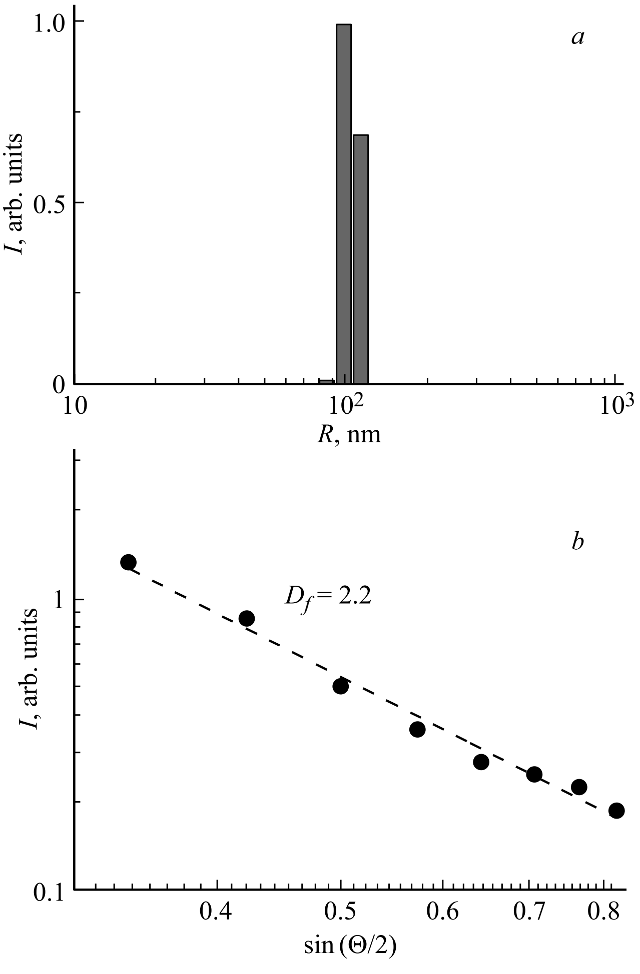

Figure 1. *a* — histogram of EMF cluster distribution over the hydrodynamic radius *R* in the stock solution; *b* — angular dependence of the normalized light scattering intensity of the EMF stock solution ($C_0 = 1.5 \cdot 10^{-5}$ M).

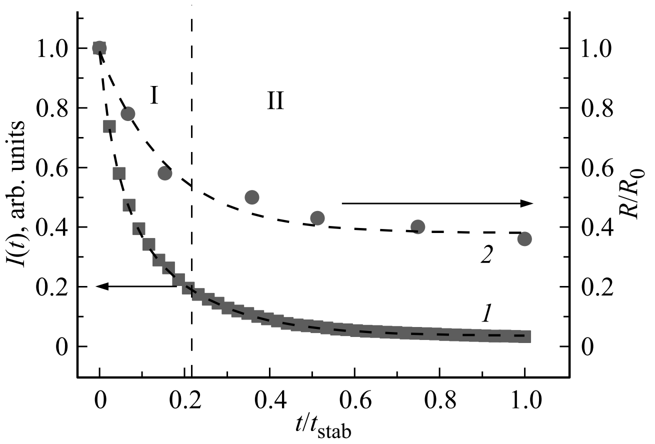

Figure 2. *1* — normalized light scattering intensity variation kinetics during EMF cluster fragmentation; *2* — hydrodynamic radii variation kinetics of EMF clusters. Region I corresponds to rapid reduction of light scattering intensity ($q^{-1} < R$). In region II, deceleration of light scattering intensity reduction is observed ($q^{-1} > R$). $R_0 = 100\,\text{nm}$, $t_{\text{stab}} = 24000\,\text{s}$.

senting the experimental data on a log-log scale, we get a set of points approximated by a straight line (Figure 1, *b*). According to (1), the slope ratio of the plot defines the fractal dimension of EMF clusters — $D_f = 2.2$.

Addition of diethylamine ($2.4 \cdot 10^{-5}\,\text{M}$) to the La@C$_{82}$ solution in DMF ($1.5 \cdot 10^{-5}\,\text{M}$) initiates the fragmentation of EMF clusters. Figure 2 shows the measurements of kinetic dependence of light scattering intensity $I(t)$ (curve *1*) and hydrodynamic radii $R(t)$ (curve *2*) during such evolution of the colloidal system.

Kinetic curve of EMF cluster radii variation (Figure 2, curve *2*) was plotted according to the maxima on the histograms of EMF cluster distribution over the hydrodynamic radii that were measured by the DLS method at various fragmentation stages. According to the obtained experimental results, relative monodispersity of the EMF cluster system was maintained during the fragmentation. A single maximum was present on all plotted histograms with radius spread of clusters within 10–15 %.

The experimental data in Figure 2 shows that there is a step-by-step reduction of the hydrodynamic radii of EMF clusters from $R \approx 100\,\text{nm}$ to $R \approx 35\,\text{nm}$ followed by thirty-fold reduction of light scattering intensity. Maintenance of the relative monodispersity of colloidal system indicates that the change of EMF cluster size results primarily from separation of single molecules or small fragments from the clusters. When the hydrodynamic radius of the EMF cluster has reached $R \approx 35\,\text{nm}$, the fragmentation stops.

Kinetic dependence of the light scattering intensity $I(t)$ shown in Figure 2 is reasonably approximated by the superposition of two exponents. The plotted kinetic curve may be conditionally divided into two regions. Region I corresponds to the rapid reduction of light scattering intensity (rapid kinetics). In region II, light scattering intensity deceleration by an order of magnitude is observed (retarded kinetics).

Transition boundary between the rapid kinetics of $I(t)$ to the retarded kinetics is marked with a dashed line in Figure 2. Point of intersection of the dashed line and kinetic curve $R(t)$ falls on the region of hydrodynamic cluster radii $R \approx 60{-}50\,\text{nm}$.

For the implemented measurement conditions (scattering angle $\theta = \pi/2$, radiation wavelength $\lambda = 654\,\text{nm}$, solvent refractive index $n = 1.493$) reciprocal scattering wave vector $q = 4\pi n \sin(\Theta/2)/\lambda$ corresponds to the scale $q^{-1} = 50\,\text{nm}$. I.e. region I corresponds to a solution consisting of large EMF clusters ($q^{-1} < R$), and region II corresponds to a solution consisting of small ($q^{-1} > R$) EMF clusters.

For fractal clusters consisting of N particles, light scattering intensity is described by the following relation [20]:

$$I(q) = N^2 P_q S_q, \tag{2}$$

where $S_q \propto (qR)^{-D_f}$ is the structural factor, P_q is the form factor that may be set to 1 or small particles with a radius much smaller than the scattered light wavelength ($\mathbf{a} \ll \lambda$).

EMF cluster fragmentation achieves plateau during $t_{\text{stab}} = 24000\,\text{s}$, the mean hydrodynamic radius of EMF clusters decreases to $R \approx 35\,\text{nm}$ (Figure 3, *a*).

For small EMF clusters ($q^{-1} > R$), the structural scattering factor may be set to $S = 1$ [21], and information about the molecular weight and fractal dimension of scattering centers may be obtained using the Debye plot. For this, concentration dependences of static light scattering in the EMF solution were analyzed at the final fragmentation stage. The method is based on the following relation:

$$\frac{KC}{R_\Theta} = \frac{1}{M_W} + 2A_2C, \tag{3}$$

where $K = 4\pi^2 n^2 (\partial n/\partial c)^2/\lambda^4 N_A$ is the optic constant; n is the refractive index of the solvent; $\partial n/\partial c$ is the refractive index increment for the solution; λ is the light wavelength; N_A is the Avogadro constant; R is the Rayleigh coefficient of the studied solution; M_W is the molecular weight of the scattering centers; A_2 is the second virial coefficient.

Refractive index increment of the EMF solution may be evaluated using equation [22]:

$$\frac{\partial n}{\partial c} = \frac{1}{\rho}\,(n_f - n_s), \tag{4}$$

where $\rho =$ is the specific density of EMF clusters, n_f and n_s are refractive indices of EMF and solution, respectively. According to [23], optical characteristics of simple and endohedral fullerenes in the wavelength range of 600–700 nm almost coincide $n_f = 2.1$ [22]. Refractive index of the EMF solution in DMF may be equated in the first approximation to the solvent refractive index. Specific density of the EMF clusters is higher than that of simple fullerenes (1.65 g/ml [22]). ρ may be corrected according to the molar weight ratio of simple and endohedral fullerenes. Then the refractive index increment of the EMF solution according to (4) is evaluated as $(\partial n/\partial c) = 0.26$ ml/g. The obtained refractive index increment coincides with that for C_{60} solution in benzene [24].

Figure 3, *b* shows KC/R_Θ vs. the EMF cluster concentration with $R \approx 35$ nm. Extrapolation of the plot to the intersection with the x axis gives the reciprocal molar weight $1/M_W$ of the clusters. From the obtained data it follows that the EMF clusters have the molar weight $M_w = 0.74 \cdot 10^7$ (g/mol). Consequently, they are formed from $N \approx 6.6 \cdot 10^3$ individual molecules. Evaluation of the fractal dimension of the EMF clusters using $N \approx (R/a)^{D_f}$ gives $D_f \approx 2.3$. Hereinafter, $a = 0.8$ nm is the effective radius of La@C_{82} molecule [25]. Positive slope of the Debye plot indicates that solvation process prevail over aggregation in the studied solution.

The results show that any significant changes of fractal dimension are not observed during EMF cluster fragmentation.

EMF cluster concentration kinetics during fragmentation was evaluated using the scaling and fractal dimension approach [21].

Intensity of light scattering by large clusters $(q^{-1} < R)$, when all monomers N_0 change to the cluster form, is described as follows [5]:

$$I(R) \propto \frac{N_0}{(R_k/a)^{D_f}}\left(\frac{R_k}{a}\right)^{2D_f}(qR_k)^{-D_f} = N_0\left(\frac{R_k}{a}\right)^{D_f}(qR_k)^{D_f}(qR_k)^{-D_f} = N_0\,\frac{1}{(aq)^{D_f}} = \text{const.} \quad (5)$$

According to (5), when all monomers change to the cluster form, we get $1/(aq)^{D_f}$-fold amplification of the light scattering signal by the EMF solution (a — is the EMF molecule radius). Thus, the light scattering intensity for the large cluster solution doesn't depend on the cluster radius, and is defined only by the fraction of clusterized EMF molecules.

For the small EMF cluster solution case $(q^{-1} > R)$, the structural factor $S_q \propto (qR)^{-D_f}$ is equal to 1 and expression (5) is written as:

$$I(R) \propto \frac{N_0}{(R_k/a)^{D_f}}\left(\frac{R_k}{a}\right)^{2D_f} = N_0\left(\frac{R_k}{a}\right)^{D_f}. \quad (6)$$

According to (6), for the small cluster case, light scattering intensity depends both on their sizes $I(R) \sim R^D$ and the fraction of clusterized EMF molecules.

Simulation of the clusterized EMF molecule fraction kinetics and then of the EMF cluster concentration kinetics during the fragmentation process is performed using the measured experimental kinetic dependences $I(t)$ and $R(t)$ (Figure 2). Intensity of light scattering by the studied EMF solution is composed of the signal from the monomer and cluster components $(I_t = I_K + I_M)$. For large $(q^{-1} < R)$ cluster solution, according to (5):

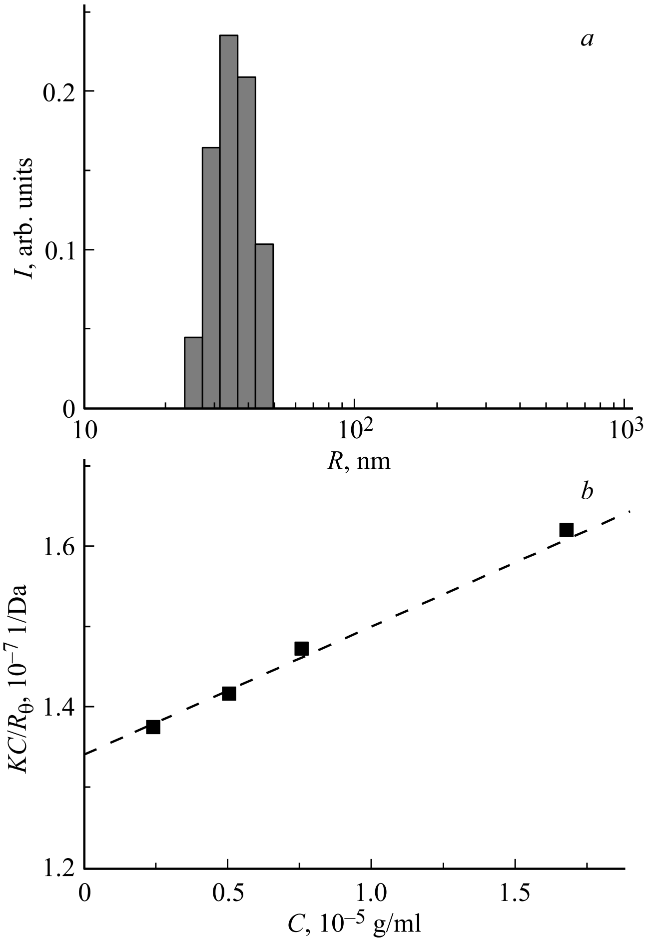

Figure 3. *a* — histogram of the EMF cluster distribution over the hydrodynamic radii for the EMF solution after completion of fragmentation; *b* — Debye plot for the EMF solution performed after completion of the fragmentation process.

$$I_K \propto \left(1 - \frac{N_M}{N_0}\right)(aq)^{-D_f}, \quad I_M \propto \frac{N_M}{N_0}.$$

Here, N_0 is the total monomer concentration, N_M is the number of nonclusterized monomers.

Then the light scattering intensity kinetics for region I (Figure 2) may be represented as follows:

$$I_t \propto \left(1 - \frac{N_M}{N_0}\right)\frac{1}{(aq)^{D_f}} + \frac{N_M}{N_0}. \quad (7)$$

For region II, small cluster solution $(q^{-1} > R)$, light scattering intensity kinetics according to (2), may be written as:

$$I_t \propto \left(1 - \frac{N_M}{N_0}\right)\left(\frac{R_k(t)}{a}\right)^{D_f} + \frac{N_M}{N_0}. \quad (8)$$

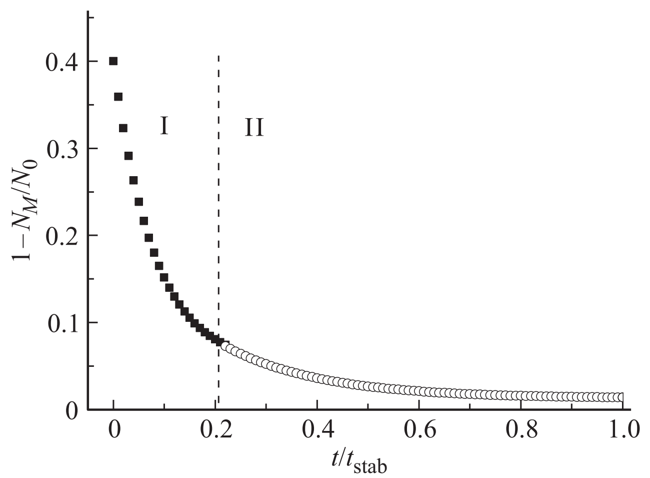

Figure 4. Clusterized La@C$_{82}$ molecule fracture kinetics during EMF cluster fragmentation. For region I, $R > q^{-1}$ is satisfied, for region II — $R < q^{-1}$ is satisfied.

The second terms on the right-hand side of equations (7) and (8) have the second order of smallness and may be neglected.

As mentioned above, the light scattering intensity for the large EMF cluster solution is defined only by the fraction of clusterized monomer component. In [5], it is shown that, for the studied La@C$_{82}$ solution in pure DMF ($R_0 = 100$ nm, $C_0 = 1.5 \cdot 10^{-5}$ M), the fraction of clusterized component is $(1 - N_M/N_0) = 0.4$.

The measurements show that, as the EMF cluster size decreases to $R = 50$ nm, the light scattering intensity is reduced by a factor of 5 (Figure 2). This corresponds to the five-fold reduction of the fraction of clusterized monomers to $(1 - N_M/N_0) = 0.08$. For region I, the light scattering intensity kinetics corresponds to the clusterized EMF molecule fraction kinetics with an accuracy to the constant multiplier:

$$I_t \propto \left(1 - \frac{N_M}{N_0}\right). \tag{9}$$

For the small cluster region ($R < 50$ nm), the clusterized monomer fraction kinetics according to (8) is determined (with an accuracy to the constant multiplier) by the ratio of the light scattering kinetics to the kinetics of monomer quantity change in the EMF cluster:

$$\frac{I_t}{\left(R_k(t)/a\right)^{D_f}} \propto \left(1 - \frac{N_M}{N_0}\right). \tag{10}$$

The normalized light scattering signal for this region varies from 0.2 to 0.03 (Figure 2).

Simulated (according to the above-mentioned data) clusterized EMF molecule fraction kinetics during fragmentation of the colloidal stock solution is shown in Figure 4.

It follows from Figure 4 that, at the final stage of the EMF cluster fragmentation in DMF solution, the clusterized molecule fraction decreases to 0.014. The mean radius of the cluster is $R \approx 35$ nm and the intensity of light scattering from the cluster component of solution is still two orders of magnitude as high as that of the monomer component of solution.

The EMF cluster concentration kinetics during the fragmentation of the colloidal stock solution is calculated by multiplying the clusterized molecule fraction by the molecule concentration in the stock solution and division by the number of molecules in the cluster with the current hydrodynamic radius $R_k(t)$:

$$N_k = N_0\left(1 - \frac{N_M}{N_0}\right)\left(\frac{R_k(t)}{a}\right)^{-D_f}. \tag{11}$$

The plot of EMF cluster concentration kinetics during fragmentation is shown in Figure 5.

According to the DLS measurements, relative monodispersity of the colloidal EMF solution is maintained during cluster fragmentation. It is unusual that the EMF cluster concentration decreases during fragmentation. Cluster fragmentation presumably takes place via transition of EMF molecules from the cluserized state to the monomer state.

The kinetic dependence curve in Figure 4 may be used to evaluate the mean number of EMF molecules leaving the cluster during fragmentation per unit time. For this, a derivative of $(1 - N_0/N_k)$ at the initial time shall be taken and normalized to the total fragmentation time, total monomer concentration and current cluster concentration:

$$\frac{d(1 - N_M/N_0)}{dt_0}\,\frac{N_0}{t_{\text{stab}}N_k} \approx 15\text{–}20. \tag{12}$$

It follows from (12) that several tens of EMF molecules on average leave the cluster per second at the start of fragmentation.

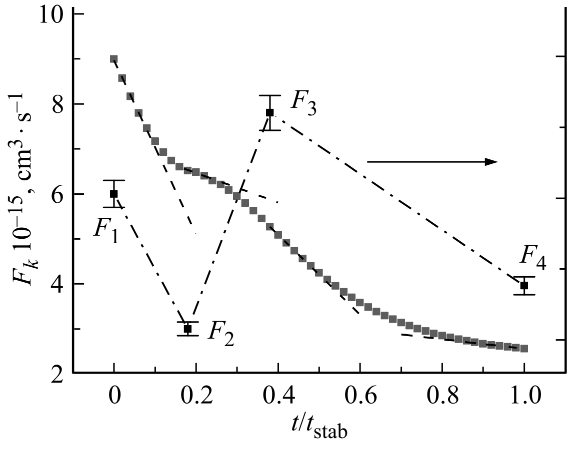

Figure 5. EMF cluster concentration kinetics during solvation. Dashed lines are tangent lines to the kinetic curve, slope ratios of which were used to evaluate the EMF cluster fragmentation rate k_F ($F_1 = 1.1 \cdot 10^{-15}\,\text{cm}^3\text{s}^{-1}$, $F_2 = 0.5 \cdot 10^{-15}\,\text{cm}^3\text{s}^{-1}$, $F_3 = 1.3 \cdot 10^{-15}\,\text{cm}^3\text{s}^{-1}$, $F_4 = 0.6 \cdot 10^{-15}\,\text{cm}^3\text{s}^{-1}$). Dashed line shows the time evolution of fragmentation rate.

Cluster fragmentation may flow spontaneously due to thermal fluctuations and collision of aggregates, when the translational energy of clusters changes to the kinetic energy of fragments. Such processes are described by the modified Smoluchowski equation [26]:

$$\frac{dN_k}{dt} = \frac{1}{2}\sum_{i+j=k} K_{i,j} n_I n_j - \sum_{i\geq 1}(K_{i,k} + F_{i,k}) n_i n_k - F_k n_k, \tag{13}$$

here $K_{i,j}$ is the aggregation rate coefficient, $F_{i,k}$ is the impact (collisional) fragmentation rate coefficient, F_k is the spontaneous fragmentation rate coefficient.

As the histograms of EMF cluster distribution over radii have no peaks corresponding to large aggregates, it is possible to neglect the aggregation process. The spontaneous fragmentation rate, other thing being equal, corresponds to the factor of the second order of smallness and, thus, can be also neglected. Then, (13) may be written as:

$$\frac{dN_k}{dt} = -\sum_{i\geq 1} F_{i,k} n_i n_k. \tag{14}$$

For the monodispersed cluster system at the initial fragmentation stage, the following may be written:

$$\frac{dN_k}{dt} = -F_k N_k^2, \tag{15}$$

here, N_k is the total number of clusters with R_k in the range of ΔR. Then:

$$-F_k = \frac{dN_k/dt}{N_k^2}. \tag{16}$$

Derivative dN_k/dt was determined as the slope ratio of tangent lines to kinetic curve $N_k(t)$ (Figure 5, dashed lines). The current cluster concentration was also found from curve $N_k(t)$.

Figure 5 shows that the curve of EMF cluster concentration N_k vs. time can be approximated by linear functions in the initial, final and intermediate segments (Figure 5, dashed lines). Expression (15) may be also used to describe individual stages of fragmentation. EMF cluster fragmentation rate coefficients F_k evaluated at various fragmentation stages according to the described scheme (Figure 5, dashed and dotted curve) vary within: $F_1 = 1.1 \cdot 10^{-15}\,\mathrm{cm^3 s^{-1}}$, $F_2 = 0.5 \cdot 10^{-15}\,\mathrm{cm^3 s^{-1}}$, $F_3 = 1.3 \cdot 10^{-15}\,\mathrm{cm^3 s^{-1}}$, $F_4 = 0.6 \cdot 10^{-15}\,\mathrm{cm^3 s^{-1}}$.

4. Conclusion

It was found that addition of diethylamine $(2.4 \cdot 10^{-5}\,\mathrm{M})$ to the La@C$_{82}$ solution in DMF initiates the fragmentation of EMF clusters. The DLS and SLS methods showed that three-fold decrease in the EMF cluster radii (from 100 nm to 35 nm) and 30-fold decrease in the intensity of light scattering by the colloidal solution take place during the fragmentation process. SLS method was used to determine the fractal dimension of EMF clusters ($D_f \approx 2.2$).

The concept of fractal dimension and scaling is behind the model representations of the dependence of light scattering intensity on effective cluster radius and EMF molecule fraction involved in clusterization. The obtained experimental data on the kinetic dependence of intensity of light scattering by the colloidal solution $I(t)$ and effective radius $R(t)$ of EMF clusters was used to plot the curves of clusterized molecule fraction and concentration kinetics $N_k(t)$ of EMF clusters during fragmentation. It was shown that cluster fragmentation was followed by the decrease in their concentration by a factor of 3.5. The fraction of clusterized EMF molecules decreases from 0.4 to 0.014.

Kinetic dependence of the EMF cluster concentration $N_k(t)$ was analyzed using the modified Smoluchowski kinetic equation. EMF cluster fragmentation rate constant at the initial fragmentation stage was determined and the time evolution of EMF cluster fragmentation rate coefficient was evaluated at various fragmentation stages.

Funding

The study was supported financially by the Ministry of Science and Higher Education of the Russian Federation: state assignment for the Federal Research Center of Problems of Chemical Physics and Medicinal Chemistry, RAS (state registration No. 124013100858-3) and state assignment for Orenburg State University No. FSGU-2023-0003 (state registration No. 123012500132-4, research topic „Alternative Physical and Chemical Methods of Pathogenic Microorganism Inactivation").

Conflict of interest

The authors declare that they have no conflict of interest.

References

[1] A.A. Popov, S. Yang, L. Dunsch. Chem. Rev. **113**, *8*, 5989 (2013).
[2] M. Mikawa, H. Kato, M. Okumura, M. Narazaki, Y. Kanazawa, N. Miwa, H. Shinohara. Bioconjugate Chem. **12**, 510 (2001).
[3] X. Lu, L. Feng, T. Akasaka, S. Nagase. Chem. Soc. Rev. 41, 7723 (2012).
[4] I.E. Kareev, V.P. Bubnov, E.K. Alidzhanov, S.N. Pashkevich, Yu.D. Lantukh, S.N. Letuta, D.A. Razdobreev. FTT **58**, *9*, 1859 (2016). (in Russian).
[5] E.K. Alidzhanov, I.E. Kareev, V.P. Bubnov, A.I. Kotov, S.N. Letuta, Yu.D. Lantukh, D.A. Razdobreev. FTT **65**, *9*, 1618 (2023) (in Russian).
[6] B.J. Olivier, C.M. Sorensen. Phys. Rev. A **41**, *4*, 20093 (1990).
[7] T.D. Waite, J.K. Cleaver, J.K. Beattie. J. Colloid Interf. Sci. **241**, 333 (2001).
[8] J. Chorover, J. Zhang, M.K. Amistadi, J. Buffle. Clays Clay Miner. **45**, 690 (1997).
[9] Y.J. Wang. Phys. Chem. **96**, 764 (1992).

[10] T. Akasaka, T. Wakahara, S. Nagase, K. Kobayashi, M. Waelchli, K. Yamamoto, M. Kondo, S. Shirakura, Y. Maeda, T. Kato, M. Kako, Y. Nakadaira, X. Gao, E.V. Caemelbecke, K.M. Kadish. J. Phys. Chem. B **105**, *15*, 2971 (2001).
[11] S.P. Solodovnikov, S.F. Lebedkin. Russ. Chem. Bull. **52**, *5*, 1111 (2003).
[12] V.N. Bezmel'nitsyn, A.B. Eletsky, M.V. Okun. UFN, **168**, 1195 (1998). (in Russian).
[13] J. Gregory. Adv. Colloid Interf. Sci. **147**, 109 (2009).
[14] D.A. Olyanich, V.V. Mararov, T.V. Utas, A.V. Zotov, A.A. Saranin. Surf. Sci. **653**, 138 (2016).
[15] V.D. Pham, V. Repain, C. Chacon, A. Bellec, Y. Girard, S. Rousset, S. Campidelli, J.S. Lauret, C. Voisin, M. Terrones, M.C. dos Santos, J. Lagoute. J. Phys. Chem. C **121**, *43*, 24264 (2017).
[16] I.E. Kareev, V.P. Bubnov, D.N. Fedutin. ZhTF **79**, *11*, 134 (2009). (in Russian).
[17] I.E. Kareev, V.M. Nekrasov, V.P. Bubnov. ZhTF **85**, *1*, 104 (2015). (in Russian).
[18] I.E. Kareev, V.M. Nekrasov, A.E. Dutlov, V.M. Martynenko, V.P. Bubnov, E. Laukhina, J. Veciana, C. Rovira. ZhFKh **91**, *3*, 492 (2017). (in Russian).
[19] K. Akiyama, K. Sueki, T. Kodama, K. Kikuchi, I. Ikemoto, M. Katada, H. Nakahara. J. Phys. Chem. A **104**, *31*, 7224 (2000).
[20] V.I. Roldugin. Uspekhi khimii **72**, *11*, 1027 (2003). (in Russian).
[21] C.M. Sorensen. Aerosol Sci. Technol. **35**, *2*, 648 (2001).
[22] Q. Ying, J. Marecek, B. Chu. J. Chem. Phys. **101**, *4*, 2665 (1994).
[23] C. Du, K. Jin, X. Liu. J. Mater. Sci. **55**, 12980 (2020).
[24] N.P. Evlampieva, S.K. Filippov, T.S. Dmitrieva, I.I. Zaitseva, E.Yu. Melenevskaya, O.V. Hazarova, E.I. Ryumtsev. Vysokom.soed. A **49**, *6*, 977 (2007). (in Russian).
[25] A. Taninaka, T. Ochiai, K. Kanazawa, O. Takeuchi, H. Shigekawa. Appl. Phys. Express **8**, *12*, 125503 (2015).
[26] V. Stadnichuk, A. Bodrova, N. Brilliantov. Int. J. Mod. Phys. B **29**, *29*, 1550208 (2015).

Translated by E.Ilinskaya